LAWRENCE
LIVERMORE
NATIONAL
LABORATORY

LLNL-TR-504971

FY11 LLNL OMEGA Experimental Programs

R. Tommasini, K. Fournier, P. Celliers, A. Comley, D. Farley, J. Hawreliak, B. Heeter, A. Kritcher, A. Lazicki, T. Ma, B. Maddox, M. May, J. McNaney, A. Pak, H. S. Park, Y. Ping, J. Ross, R. Rygg, V. Smalyuk, R. Smith, G. W. Collins, W. Hsing, O. Landen

October 12, 2011

Disclaimer

This work performed under the auspices of the U.S. Department of Energy by Lawrence Livermore National Laboratory under Contract DE-AC52-07NA27344.

LAWRENCE
LIVERMORE
NATIONAL
LABORATORY

LLNL-TR-504971

FY11 LLNL OMEGA Experimental Programs

R. Tommasini, K. Fournier, P. Celliers, A. Comley, D. Farley, J. Hawreliak, B. Heeter, A. Kritcher, A. Lazicki, T. Ma, B. Maddox, M. May, J. McNaney, A. Pak, H. S. Park, Y. Ping, J. Ross, R. Rygg, V. Smalyuk, R. Smith, G. W. Collins, W. Hsing, O. Landen

October 12, 2011

FY11 LLNL OMEGA Experimental Programs

TABLE OF CONTENTS:

FY11 LLNL OMEGA Experimental Programs

In FY11, LLNL conducted several campaigns on the OMEGA laser system and on the EP laser system, as well as campaigns that used the OMEGA and EP beams jointly. Overall LLNL led 294 target shots involving the OMEGA laser system and 82 target shots involving the EP laser system. Approximately 35% of the total number of shots (126 OMEGA shots, 10 EP shots) shots supported the National Ignition Campaign (NIC). The remainder was dedicated to experiments for High-Energy-Density Physics (HED) (168 OMEGA shots, 72 EP shots).

Objectives of the LLNL led NIC campaigns at OMEGA included:

The LLNL led HED campaigns covered four main areas of research:

This work performed under the auspices of the U.S. Department of Energy by Lawrence Livermore National Laboratory under Contract DE-AC52-07NA27344.

National Ignition Campaign Experiments

Characterization of long-pulse, high-resolution, laser-produced backlighters (3wCR - PI: R. Tommasini)

In FY10 we characterized short-pulse Bremsstrahlung backlighters produced by 10ps, 1ω, laser pulses from the OMEGA EP laser. Using these pulses, we successfully demonstrated Compton Radiography of direct drive implosions of spherical shells and of cone-in shells. The last type of targets is of interest for fast ignition.

In FY11 we characterized long-pulse Bremsstrahlung backlighters produced by 100ps, 3ω, laser pulses from the OMEGA laser. These x-ray sources are of interest for the earliest implementation of Compton radiography on the NIF. [Ref .1: Tommasini et al. Phys. Plasmas (2011) vol. 18 (5) pp. 056309]. The backlighters were produced overlapping up to 18, 100ps 3ω laser beams of OMEGA, of total power ~ 8TW to match or exceed single NIF 3ω quad intensities, onto 300um long, 10 um-diameter Au microwires.

The conversion efficiency of the backlighters, into 70-200 keV X-rays, was measured using an annular step-wedge filter hosted in the custom-built Compton Radiography Snout (CRS). Figure-1 shows a comparison of the conversion from 1ω-10ps (dots) and 3ω-100ps (squares) laser-produced 10-um-diameter Au backlighters. The latter type of targets gives conversion efficiencies between 1e-5 and 3e-5, in the available intensity range 310^{16}-$1x10^{17}$ W/cm^2. As we have observed, these conversion efficiencies

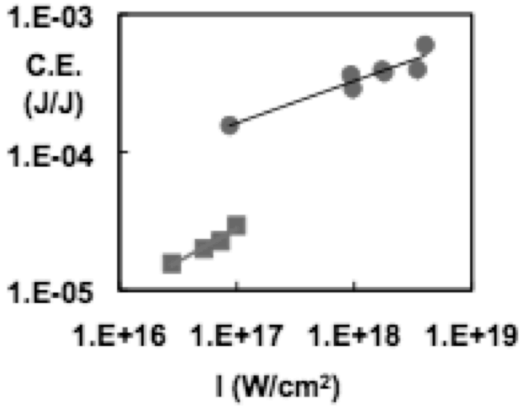

Figure A: *Conversion efficiency as a function of laser intensity into 70-200 keV X-rays from 1ω-10ps (dots) and 3ω-100ps (squares) laser-produced 10 um-diameter Au backlighters.*

are typically a factor of 7-10 less than for planar foil targets and consistent with the ratio of wire area to laser spot area. They are also ≈7x less than for 1ω sources at the same intensity, ascribed to the $I\lambda^2$ dependence of hot electron production. Such efficiencies at 3ω should be sufficient to measure fuel areal densities and radii to 7% accuracy at 20 μm spatial scales on NIF, and observe 20% fuel areal density and shape non-uniformities up to mode 4.

The source size of the 3ω backlighters was measured by fitting experimental radiographic transmission lineouts of tungsten-carbide spheres to simulated radiographs for Gaussian-shaped sources using the spectra measured by the CRS step-wedge. This method resulted in typical Gaussian FWHM source sizes of (11 ± 2) μm, in all cases close to the diameter of the Au wires. The pulse durations were

inferred from an X-ray streak camera measuring the emission from Au in the spectral region above 3keV, to be 100 ± 5 ps.

[1] Tommasini et al. "Development of Compton radiography of inertial confinement fusion implosions." Phys. Plasmas (2011) vol. 18 (5) pp. 056309

4ω Thomson Scattering (4wTS – PI: S. Ross)

4ω Thomson scattering measurements were made from foil (shown in Figure 1) and hohlraum targets to determine plasma conditions. Figure 2 shows the measurement of Thomson scattering from the ion-acoustic wave (ion feature) and the electron-plasma wave (electron feature) resonances using a 4ω probe beam from a CH foil target. From the scattered spectra the electron density, temperature, plasma flow velocity, and ion temperature is measured.

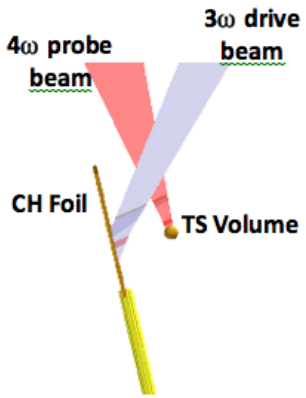

***Figure 1**: The foil target configuration is shown.*

Measurements from foil targets produced excellent data. Hohlraum targets proved more difficult due to the complex target geometry, which produced increased background and inhibited probe beam propagation. The Thomson scattering diagnostic was activated successfully and the measurements made from foil and hohlraum targets will be used to improve experimental and diagnostic design for upcoming experiments planned for FY12.

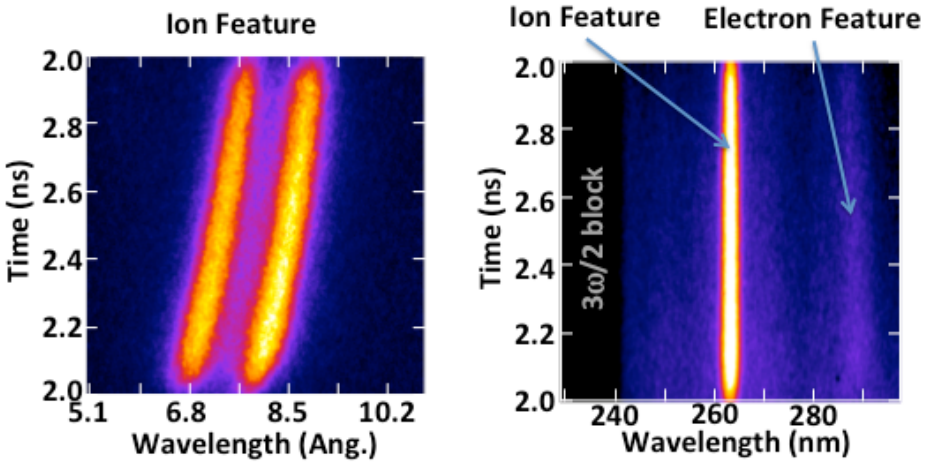

Figure 2: Streaked Thomson scattering data from the ion-acoustic wave and electron-plasma wave resonances.

Neutron-induced backgrounds for ARIANE (ARIANE - PI: V. Smalyuk)

X-ray imaging instruments will operate in a harsh ionizing radiation background environment on implosion experiments at the National Ignition Facility (NIF). These backgrounds consist of mostly neutrons and gamma rays produced by inelastic scattering of neutrons. The experiment was designed to measure these backgrounds generated in some of the components of x-ray framing cameras used in the ARIANE imaging system; phosphors, fiber-optic plates, and T-MAX 3200 film. The experiment consisted of 6 implosions with 1.5-mm outer diameter, 4-μm thick glass shells filled with 5 atm of DT gas, driven with 60 OMEGA beams with total UV energy of ~28 kJ. Measured DT neutron yields were in the range from ~3e13 to ~4e13. Fiber-optic plate samples were coated with five different phosphors (P-11, P-20, P-43, P-46, and P-47), and placed in the OMEGA target chamber at ~21 and ~42 cm from chamber center. Neutron-induced background signals were detected on T-MAX 3200 film. Figure 1 shows an example of the film data, with measured backgrounds in P-43 phosphor, fiber-optic plate, and film (lighter area); and with film only (darker area). Figure 2(a) shows the background intensity as a function of DT neutron exposure measured in P-43 phosphor, fiber-optic plate, and film (diamonds with exponential fitting shown with a solid curve); and in film only (triangles with exponential fitting shown with a dashed curve). Figure 2(b) shows backgrounds in fiber-optic plate with a film (diamonds), and in film only (triangles). Measured total backgrounds in samples with P-11, P-46, and P-47 phosphors were similar, with ~50% generated in film, ~20% in fiber-optic plates, and ~30% in phosphors. The total backgrounds generated in both P-20 and P-43 phosphors were about factor of 1.5 larger than in samples with P-11, P-46, and P-47 phosphors. Based on these measurements, the maximum peak signal is predicted to be about 5 times higher than the background for an ARIANE framing camera using P-11 phosphor and film for NIF shots with DT yields of 4e16. Such a background will be manageable for measurements of the shape of the implosion core.

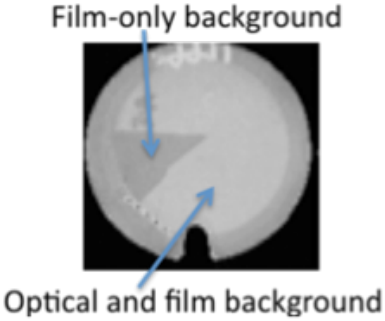

Figure 1. *Measured optical backgrounds in P-43 phosphor, fiber-optic plate, and film (lighter area); and with film only (darker area).*

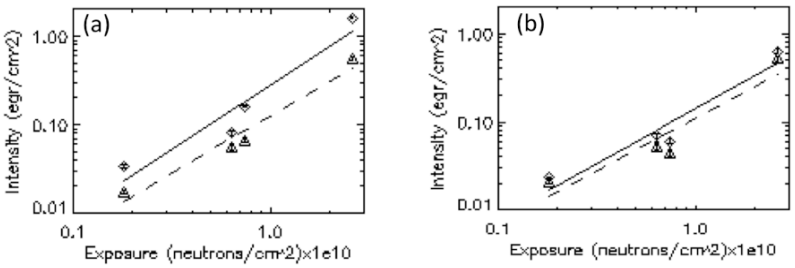

Figure 2. *(a) Background intensity as a function of DT neutron exposure measured in P-43 phosphor, fiber-optic plate, and film (diamonds with exponential fitting shown with a solid curve); and in film only (triangles with exponential fitting shown with a dashed curve). (b) Backgrounds in fiber-optic plate with a film (diamonds), and in film only (triangles).*

Thermal conductivity measurements at a heated CH/Be interface by refraction-enhanced x-ray radiography (AtwoodNum - PI: Y. Ping)

This is a new series of campaigns aiming at thermal conductivity measurements at CH/Be interface under conditions relevant to NIC design, where the Be is a surrogate for DT. A novel technique, refraction-enhanced slit projection x-ray radiography, was successfully implemented to measure the evolution of the density profile at a cylindrical CH/Be interface which was isochorically heated by Ag L-band 3 keV radiation. High-quality radiographs enabled us to determine the density gradient near the CH/Be interface from the fringe contrast with 2 μm-level accuracy, from which the thermal conductivity will be inferred. In addition to observation of the expected density evolution caused by thermal conduction, counter-propagating shock and rarefaction waves were also observed, and their velocities were measured simultaneously. The multiple observables with the same diagnostic will strongly constrain the EOS of CH/Be and the temperatures after heating. A technical paper based on this campaign has been published (Y. Ping et al. J. Inst. 6, P09004, 2011), and data are being analyzed to benchmark the transport models in NIC design codes. In FY12 this experimental design will be extended to include cryogenic cells for measuring thermal conductivity of D2, which is critical for assessing hydro-instability margins during ICF implosions.

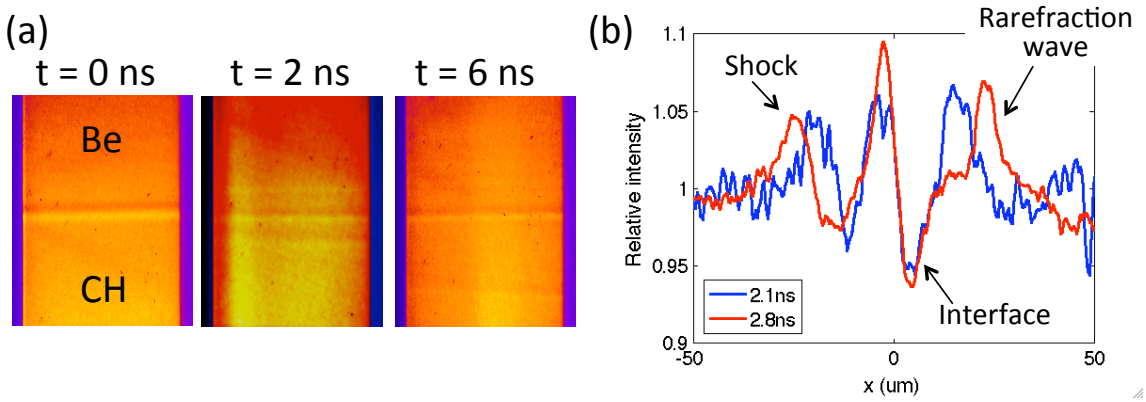

Figure 1: (a) 5.4 keV radiographs at t= 0, 2 and 6ns. (b) Lineouts of two frames taken in one shot, showing the shock wave and rarefaction wave counter-propagating from the interface.

18 keV X-Ray Thomson Scattering of Shock Compressed Beryllium & Aluminum (BeXRTS – PI: T. Ma)

The accurate characterization of material properties under extreme conditions is an important issue for the understanding of high energy density states of matter. We performed two experiments on OMEGA in FY11 in which spectrally resolved x-ray Thomson scattering at 18 keV was used to determine the electron density and temperature of shocked Be and Al. 125-um solid beryllium and aluminum targets were shock compressed to high density (>3x solid density) using 9 beams with a total energy of 4.5 kJ in a stacked 1 ns or 3 ns configuration. SG4 distributed phase plates were used to achieve a smooth 800-um focal spot, yielding a total drive intensity of $3x10^{14}$ W/cm^2 on the sample.

The materials were probed in the noncollective scattering regime using Mo 2-1 line radiation x-rays at ~17.9 keV. In the first portion of the campaign (BeXRTS-11A), the scattering angle was held constant at 90°, while scattering was performed on undriven and driven Be and Al.

In the case of beryllium scattering, both the driven and undriven cases showed as expected depressed elastic scattering attributed to the ionization potential of Be electrons being less than the Compton energy ≈ 600 eV. Fits to the ratio of elastic to inelastic peaks for the undriven data gave a Z of ~1.5-2 (see Fig. 1b), in agreement with Ref. 1. In the case of Al, the unshifted Rayleigh scattering increased when driving the Al sample, attributed to increased disorder in the heated lattice (see Fig. 1c). It was found that the ratio of the elastic to inelastic scattering features in the shocked Al were very sensitive to the ionization potential of the L-shell electrons (when Compton Energy > Ionization Potential of L-shell electrons, these electrons contribute in the same way as free electrons, and only the two K-shell electrons will Rayleigh scatter).

For the last series BeXRTS-11B, Mo 2-1 line radiation was again employed as an x-ray probe while the scattering angle was varied from 25°– 155° (Compton energy from 60 eV – 1.2 keV). This allowed us to assess the sensitivity to continuum lowering and measure the angularly resolved strength of the static structure factor. Experimental data was found to corroborate the code predictions: at smaller scattering angles, the Compton feature was merged into the Rayleigh, while the relative strength of the inelastic feature grows at higher scattering angle.

[1] H. J. Lee *et al.*, Phys. Rev. Lett. **102**, 115001 (2009).

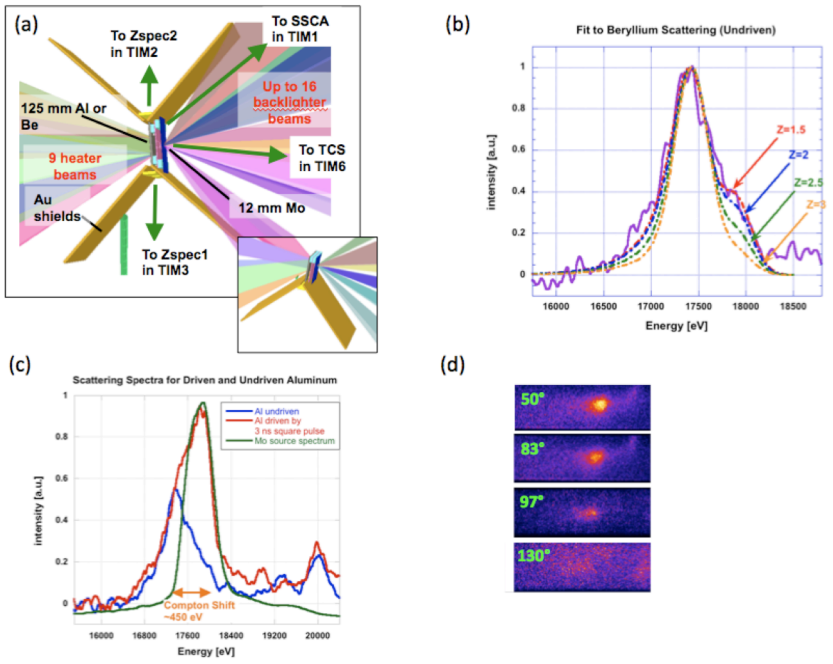

Figure 1: (a) The experimental configuration for BeXRTS-11B. Inset shows the single-wing, 90 degree configuration used in BeXRTS-11A (b) Fits to the undriven beryllium scattering vs Z. (c) Comparison of source spectrum (green), undriven (blue) and driven Al (red) scattered spectra. (d) Al scattering vs increasing scattering angle (scattering k).

High-resolution measurements of velocity nonuniformities created by microscopic perturbations in NIF ablator materials (CAPSEED – PI: P. Celliers)

This campaign focused on three aspects of NIF ablators: continue the survey of Rev5 Ge-doped CH samples (7 shots), continue the survey of diamond samples near the melt curve (2 shots) and perform the first test measurements of double-shocked diamond samples (2 shots). For the CH samples we also tested a simplification of the target design in which the shock was transmitted from the ablator directly into the fused silica window instead of the polymethylmethacrylate (PMMA) layer that was used in previous designs. The results showed that the shock front reflectivity in the fused silica window is too low to produce high quality data, so future designs will continue to use the PMMA layer to capture the shock front non-uniformities. The two single shock experiments on diamond samples were designed to probe into the shock melt region (about 600 GPa), and the results confirmed that partial shock melting produced much smoother shock fronts than lower amplitude shocks that do not melt the sample. Finally, the two shots on double-shocked diamond were performed to test the drive and measure timing

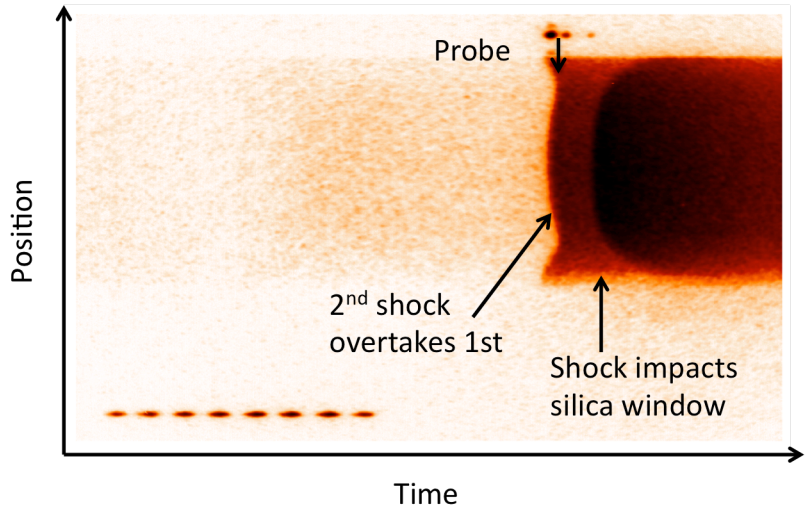

Figure 1: Streak record showing the second shock overtake and OHRV probe timing for a two-shock drive applied to a non-crystalline diamond ablator sample.

information in preparation for a more extensive future series. On the first shot the second shock overtake was clearly observed, however the probe was synchronized too early to capture the second shock overtake event. For the second shot the probe was adjusted to capture the data just after the second shock overtook the first. On this shot we recorded the first data on shock-front perturbations from double-shocked diamond. This information will be used to design a more comprehensive future campaign to assess diamond ablators up to the second shock level.

X-Ray Thomson Scattering of Shock Compressed Beryllium on OMEGA EP (EPXRTS – PI: A. Pak)

This year, two shot days with a total of ten laser shots were used to study laser shock compressed beryllium using non-collective x-ray Thomson scattering (XRTS) at OMEGA EP. The primary goal of the EPXRTS 11A campaign was to develop a suitable experimental platform to study laser shock compressed matter with XRTS. Four laser shots were taken, testing two scattering targets and two drive conditions. Only one of the scattering targets produced a scattering signal shown in Fig. 1. The goal of the second shot day (EPXRTS 11B) was to use non-collective XRTS at two scattering angles to measure the change in the temperature of the shocked beryllium as the laser drive pulse shape was changed from a super Gaussian shape to a ramped adiabatic shape. Again four shots with two scattering targets were taken, but a clean scattered spectrum was not measured from this campaign. It is thought that a change in laser beam configuration prevented the successful scattering target from EP-XRTS 11A from producing a scattered signal. The second scattering target, which was modified to reach smaller scattered angles, allowed for un-scattered x-rays to reach the detector preventing a clean scattered signal from being measured.

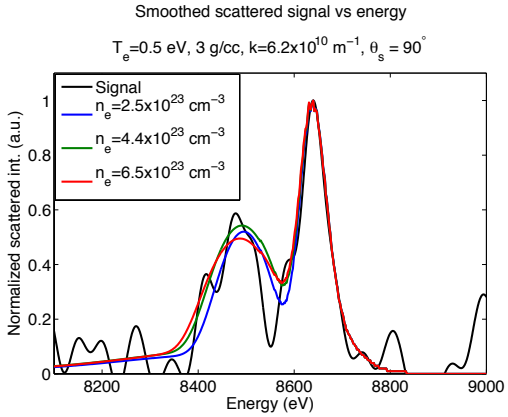

Figure 1: Measured scattered signal from EP-XRTS 11A (black) vs scattered energy. Here Zn - Kα x-rays at 8.64 keV elastically and inelastically scatter though a Be target that has been shocked by a laser with an $I_o \approx 1x10^{13}$ W/cm^2. Three theoretical scattered spectra are plotted vs energy as a function of density, at a fixed temperature and scattering angle.

Pb Hohlraums (PbHohlraum - PI: S. Ross)

A comparison of Pb and Au hohlraums shows very similar performance for three shaped laser pulses. The point design for Laser Inertial Fusion Energy (LIFE) targets relies on Pb for the primary hohlraum material. Lead and gold hohlraums are predicted to have similar performance and these are the first measurements to validate those predictions. The hohlraum performance was measured using Dante to determine the hohlraum radiation temperature (Figure 1) and FABS to measure the backscattered energy. Both diagnostics show no measureable difference between Pb and Au.

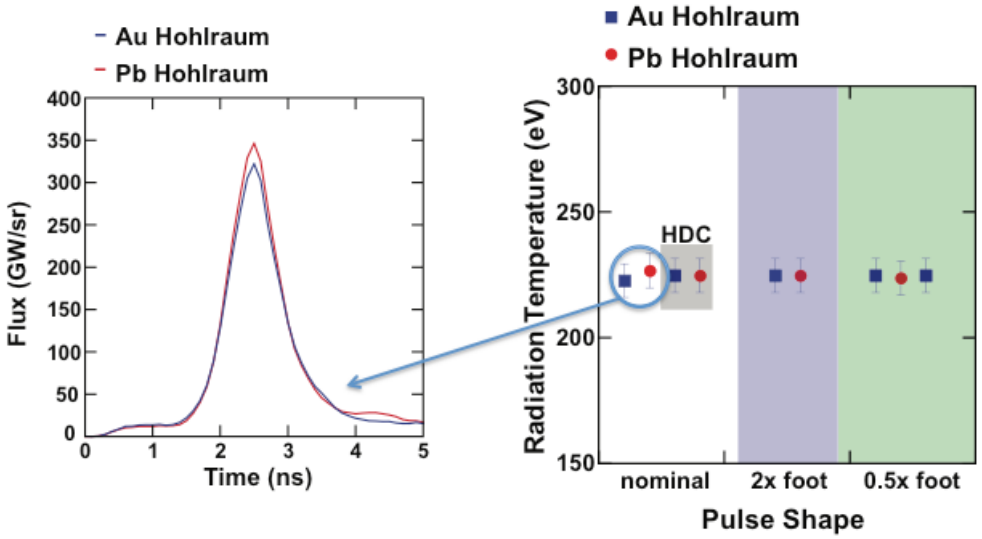

Figure 1: *Time resolved Dante flux and peak radiation temperature for Pb vs. Au hohlraums.*

Neutron yield (shown in Fig.2) was also used to assess hohlraum performance and again Pb and Au hohlraums produced very similar results. These experiments are a successful first step in validating Pb as a viable hohlraum material for a LIFE point design target.

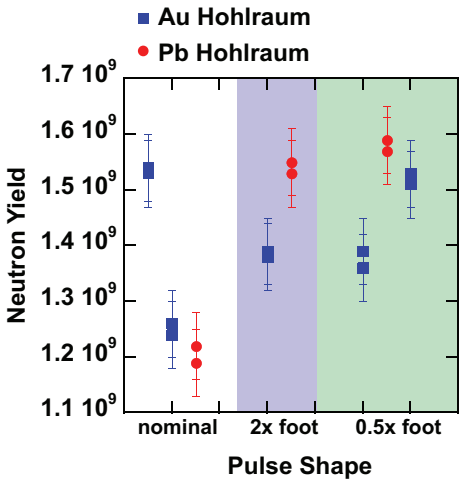

Figure 2: *The neutron yield is compared for 3 pulse shapes for the Au and Pb hohlraums.*

Surrogate Mix Targets with Dual Backlighting (TwoColorBL – PI: D. Farley)

A half day of experiments were conducted on OMEGA on 13 January 2010 to test two-color radiography of surrogate mix samples as a means of assessing both density and concentration. The backlighters and surrogate mix materials were paired so the backlighter resonance line energies straddled the K edge of one material while both energies stayed either below or above the K edge of the other material. One type of surrogate mix target used Cu and Ge thin foils mounted on a CH block, which was backlighted separately by Cu (8.4 keV), Ge (9.6 keV) or Zn (9.0 keV) backlighter materials (see Fig. 1). This type of surrogate mix target simulates dopant levels at peak velocity for Ge- and Cu-doped plastic capsules. The other type of surrogate mix target consisted of Si and Ge foils mounted on the same size block of CH as before, to simulate Si and Ge dopants in a CH capsule, paired with Cu and Zr backlighters. Since Zr Helium-like emission peaks at ~16.4 keV, it should transmit through Si-doped

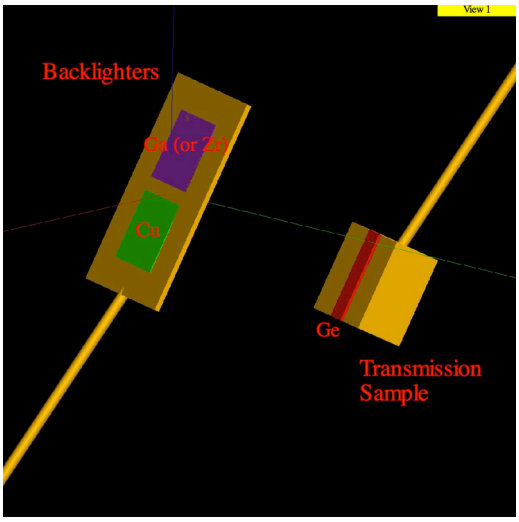

Figure 1. *Setup of the experiment showing dual backlighters and mix target (Si or Cu on back side of transmission sample – not shown). The mix foils overlap ~100 μm when viewed face-on by camera.*

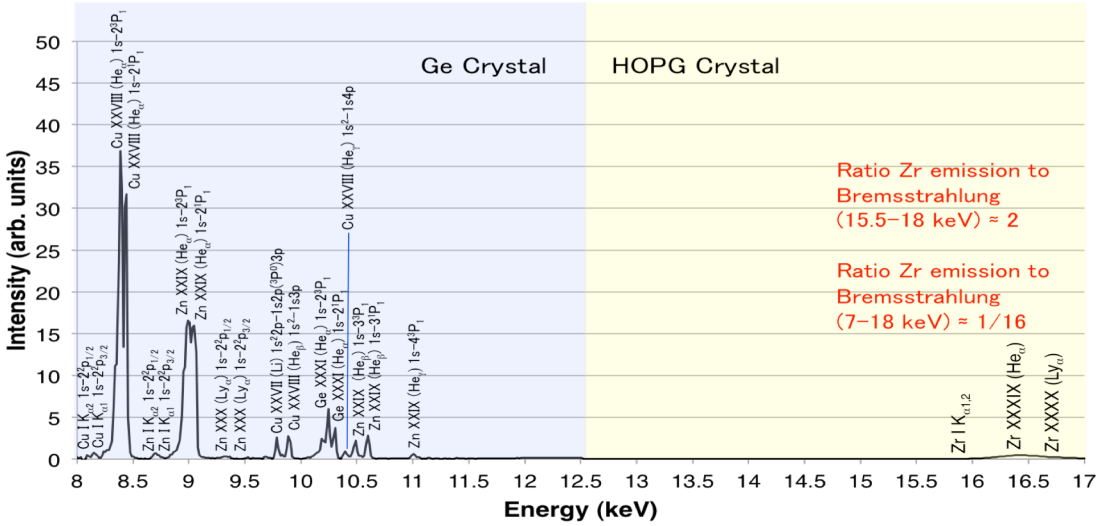

Figure 2. *Collected spectra from TwoColorBL experiment backlighters, scaled by laser energy that was applied to each foil material. CEA XCCS spectrometer was used.*

CH slightly better than Ge-doped CH with no noticeable transmission difference in the overlapped Si/Ge foil region, but there should be an observable change in transmission in the Si/Ge (or Cu/Ge) 100 mm overlapped region for the 8.4 keV Cu backlighter emission. Thus, comparison of the transmission

profiles of the two backlighters would provide an indication of mix width. However, the Zr laser to x-ray conversion efficiency will be quite low.

C. Reverdin and F. Girard from CEA assisted in these experiments through providing diagnostic support for their CEA XCCS spectrometer, which had the spectral range to cover the Zr emission up to ~17 keV. A collection of spectra from the XCCS spectrometer is shown in Fig. 2. From this spectral result, the Zr conversion efficiency was estimated at 0.04%, at least 10x lower than for Cu. The transmission profile for the Cu backlighter through the simulated mix sample was as expected. Further work is needed to determine the best dopant-backlighter pairing, but clearly we would have preferred a lower Z such as As or Se if feasible.

High-Energy-Density Experiments

I. Material Dynamics and Equation-of-state

Kr Hugoniot measurements to 730 GPa (CO2XeEOS-11A/B/C, PI Ryan Rygg)

Experimental measurement of the Kr Hugoniot was extended up to 730 GPa by launching shocks into Kr samples pre-compressed in diamond anvil cells to ~0.5 GPa. VISAR and SOP measurements of the Kr shock front in comparison to concomitant measurements in quartz were used to infer pressure, density, reflectance, and temperature of shocked Kr. In addition, Hugoniot measurements on solid CO_2 pre-compressed to 1.0 GPa were compared to previous liquid CO_2 measurements to infer Gruneisen Γ of 0.5 and isochoric specific heat of 4.0 k_B/atom for CO_2 ρ, T of 4.5 g/cc, 4 eV.

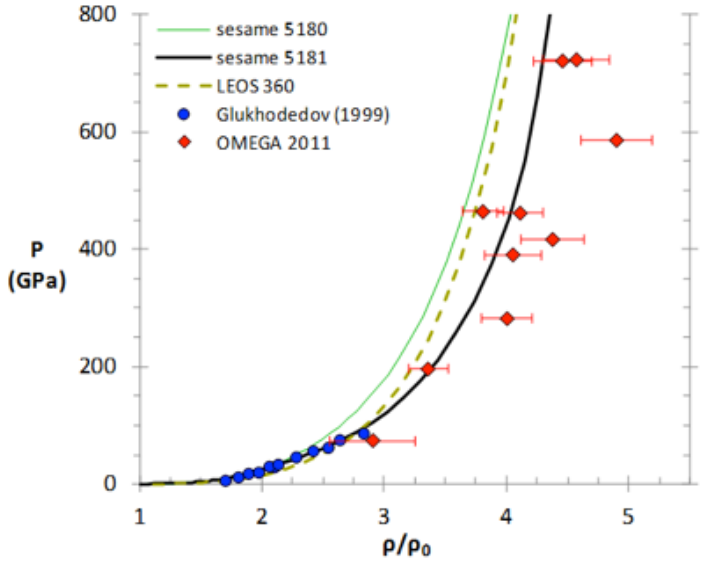

***Figure 1**. Previous experimental measurements of the Kr Hugoniot (open markers) reached 87 GPa. In FY11, the OMEGA laser was used to extend the range to 730 GPa (filled diamonds). The Kr shock pressure and density were inferred by shock velocity measurements impedance matched to a quartz standard*

Ramped Compression of Different Materials (RampComp-11A/B/C, PI Ray Smith)

The goal of the RampComp-11A shots was to measure the stress-density response of a nano-diamond step target through an indirect-drive ramp compression technique. As shown as insert to Figure 1 the target geometry consists of an Au hohlraum with a multi-stepped diamond sample attached to the back. The target was aligned on the H7-H14 axis on Omega. Fifteen beams with 300 μm elliptical phase plates inserted into the beamlines were focused onto the inner walls of the hohlraum. We used a 3.5ns ramp laser profile (rm3502) to generate a time-dependent x-ray temperature, which translates into a ramped longitudinal stress wave propagating through the stepped diamond (30/35/40/45 μm) target. The primary diagnostic was the ASBO (VISAR), which records the free-surface velocity as a function of time, $u_{fs}(t)$, for each step. Following a Lagrangian sound speed analysisi the stress-density response is calculated from the $u_{fs}(t)$ record and shown as the red curve in Fig. 1. Also shown are previously reported ramp compression data of Bradley[1] on micro-grain data and statically compressed data of Occelli[2].

1

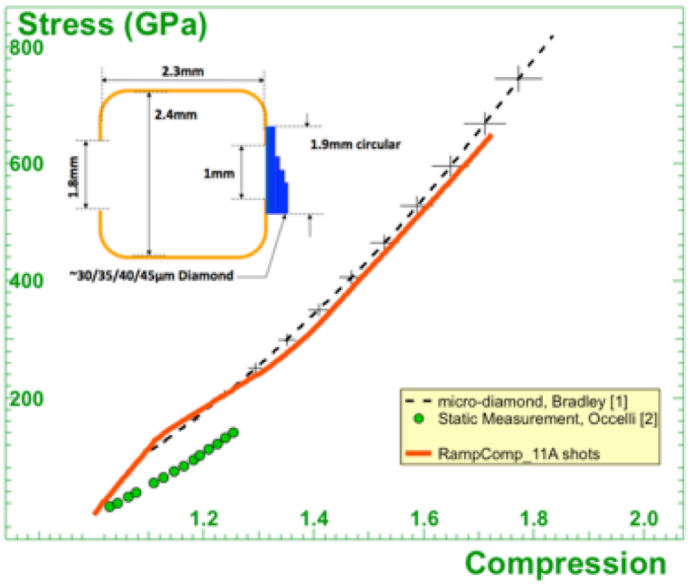

Figure 1. *Stress-density response of a 200nm grain size nano-diamond sample (red curve). This is an average of seven shots from the RampComp_11A series. Also shown is previous ramp compression data from Bradley[1] on micro-grain diamond and static measurements from Occelli[2]. Shown as insert is the target geometry for the RampComp-11A shot series.*

The goal of the RampComp-11B shots was to measure the stress-density response of a Ta step target through an indirect-drive ramp compression technique. As shown as insert to Figure 2 the target geometry consists of a Au hohlraum with a multi-stepped Ta sample (with 20 μm diamond ablator) attached to the back. The target was aligned on the H7-H14 axis on Omega. Fifteen beams with 300μm elliptical phase plates inserted into the beamlines were focused onto the inner walls of the hohlraum. We used a 3.5ns ramp laser profile (rm3501) to generate a time-dependent x-ray temperature, which translates into a time-dependent ablation of a 20μm diamond ablator. This results in a ramp longitudinal stress wave propagating through the stepped Ta (6/8/10/12 μm) target. The primary diagnostic was the

ASBO (VISAR), which records the free-surface velocity as a function of time, $u_{fs}(t)$, for each step (Fig. 1). On the RampComp_11B series we had seven shots in a half-day. Using a Lagrangian sound speed analysis technique[1] we can extract the stress-density response of Ta to 3 Mbars. This data is currently being prepared for publication.

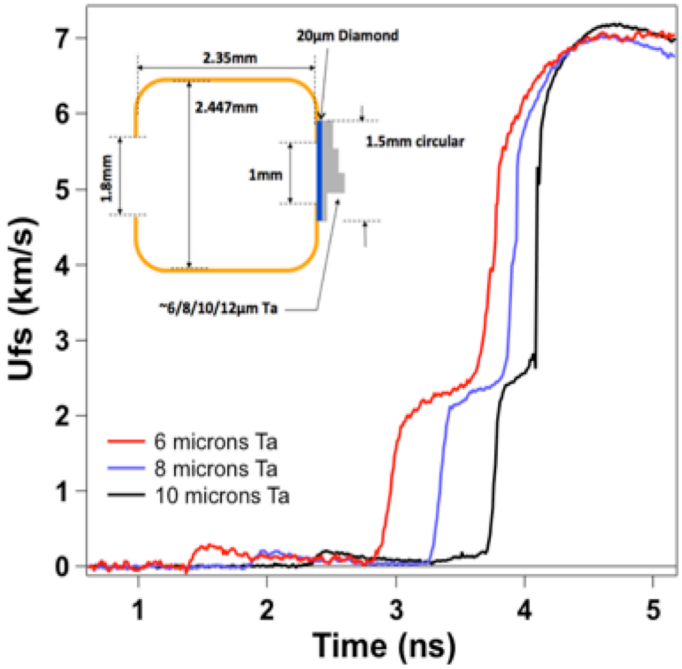

Figure 2. *Free-surface velocity versus time, $u_{fs}(t)$, for three different thicknesses of Ta. The low velocity precursors are a result of laser glint of hohlraum walls being absorbed at the diamond-Ta interface. The ramped plateau initiated at ~2 km/s is from the transmitted diamond elastic wave.*

The goal of the RampComp-11C shots was to measure the stress-density response of Fe through an indirect-drive ramp compression technique. The target geometry consists of a Au hohlraum with a multi-stepped diamond sample attached to the back. The target was aligned on the H7-H14 axis on Omega. Fifteen beams with 300μm elliptical phase plates inserted into the beamlines were focused onto the inner walls of the hohlraum. We used a composite laser pulse shape with six beams in the rr1901 pulse to launch a 70GPa shock into the sample followed 2ns later by nine beams with the rm4002 pulse shape to ramp compress to ~300GPa. The time-dependent laser power results in a time-dependent longitudinal stress wave propagating through the Fe. The primary diagnostic was the ASBO (VISAR), which records the free-surface velocity as a function of time, $u_{fs}(t)$, for each step. Following a Lagrangian sound speed analysis[1] the stress-density response is calculated from the $u_{fs}(t)$ record and shown as the red curve in Fig. 3. Also shown are previously reported shock compression and static measurements from Dewaele[3] and Dubrovinsky[4].

[1] D.K. Bradley, J.H. Eggert, R.F. Smith, S.T. Prisbrey, D.G. Hicks, D.G. Braun, J. Biener, A.V. Hamza, R.E. Rudd, and G.W. Collins, Phys. Rev. Letts. **102**, 075503 (2009).
[2] F. Occelli, P. Loubeyre, and R. Letoullec, Nature Mater. **2**, 151 (2003).

[3] A. Dewaele, P. Loubeyre, F. Occelli, M. Mezouar, P. I. Dorogokupets, M. Torrent, Phys. Rev. Lett. **97**, 215504 (2006).
[4] L. S. Dubrovinsky, S. K. Saxena, F. Tutti, T. Le Bihan, Phys. Rev. Lett. **84**, 1720- 1723 (2000).

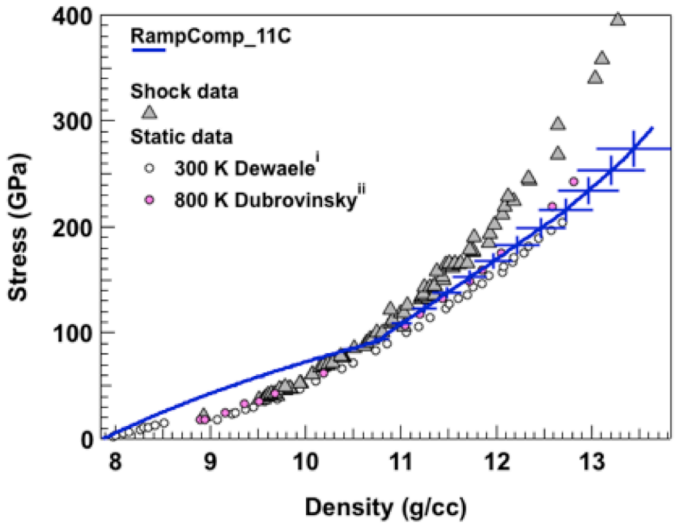

***Figure 3**: Stress-density response of Fe (blue curve). This is an average of six shots from the RampComp_11C series. Also shown are previous shock compression data and static measurements from Dewaele[2] and Dubrovinsky[3].*

Tin Melt (TinMelt-11A, PI James McNaney, Amy Lazicki)

During the April 2011 Tin melt campaign, we shocked and/or ramp compressed tin prepared in diamond-tin-diamond or diamond-tin-LiF sandwich targets, while measuring particle velocities, powder x-ray diffraction and temperature using the VISAR, PXRDIP and SOP diagnostics. One purpose of the campaign was to probe for high-pressure solid crystalline phases using pure ramp compression in order to extend the solid equation of state to higher pressure, and to look for new phase transitions. We were able to exceed 200 GPa on multiple shots, and we see a shift in the dominant diffraction peak and the appearance of new features, indicating a phase transition (Figure 1, compared with known diamond anvil cell results[1]). The second purpose of the campaign was to begin exploration of the tin melting curve by creating a pulse shape that would shock-melt tin followed by a ramp compression back across the melting curve, measuring x-ray diffraction at the end of the ramp to confirm recrystallization. We succeeded in generating a shock followed by a ramp to the desires pressures, and we observed a plateau in the velocity profile consistent with a phase transition such as recrystallization (Figure 2) . We also observe x-ray diffraction features that appear crystalline, indicating that the phase boundary back to the solid has been crossed within the time scale of the experiment. Work is ongoing to verify these observations and to explore the solid to higher pressures and the melting curve to higher temperatures.

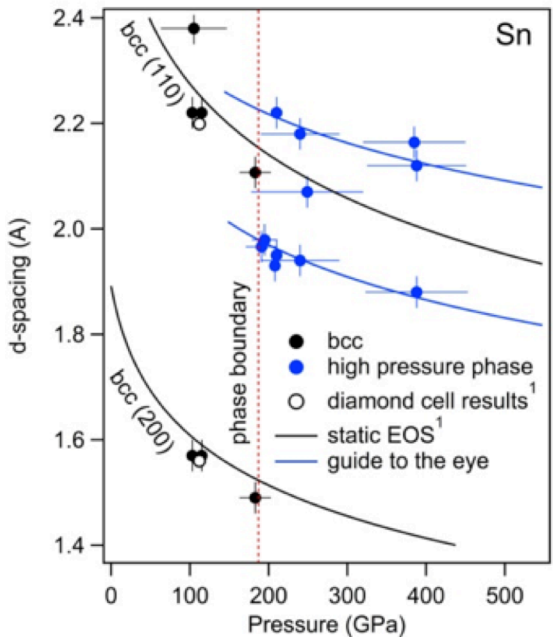

Figure 1. *Pressure-induced shift in d-spacing of different peaks compared to static diamond anvil cell results.*

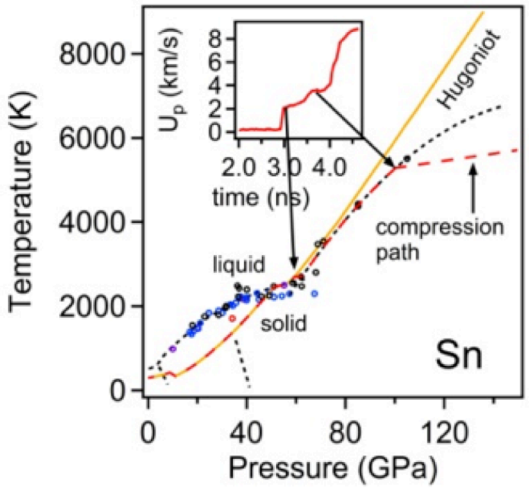

Figure 2. *Melting curve of Sn with suggested compression path corresponding to observed velocity profile (shown in inset)*

[1] Desgreniers et al., Phys. Rev. B 39, 10359 (1989).

Powder x-ray diffraction measurements of solid Fe and Ta to 570 GPa (RampDiff-11A/B, PI Ryan Rygg, James Hawreliak)

The OMEGA powder x-ray diffraction platform has been further refined in FY2011 to obtain diffraction results on solid samples at pressures above Hugoniot melt, including the first detection of the highest solid-solid phase transition to date (to our knowledge). Fe and Ta samples were sandwiched between a diamond pusher and window, and ramp-compressed to high pressure and density using up to 6 beams. VISAR velocity measurements were used to infer the pressure history in the sample, and the 8.37 keV Cu-He$_\alpha$ x-ray source, driven by 10 beams, was timed to coincide with the peak pressure. The diffraction signal is collimated through a 300-μm-diameter aperture, and captured on image plate detectors. Density is inferred from the diffraction data by assuming a crystal structure, then verifying self-consistency with a best fit to density. Fe diffraction measurements were consistent with HCP phase up to 570 GPa, and an extra peak observed in Ta above 340 GPa is consistent with a phase transition from BCC to ω-phase.

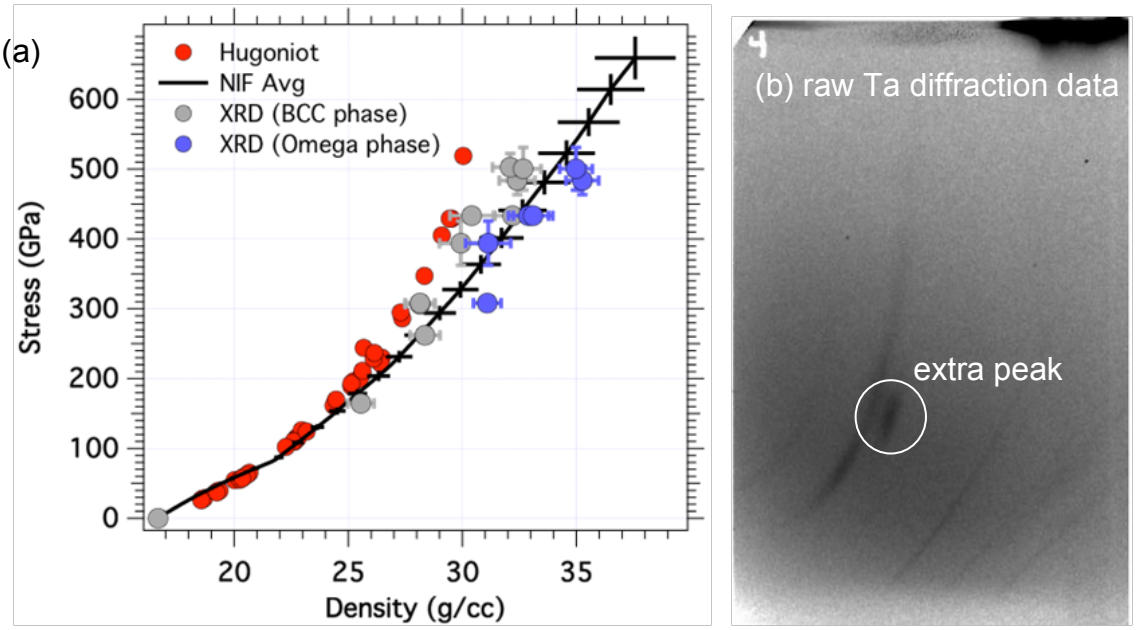

Figure 1. *(a) Stress-density of tantalum, where x-ray diffraction (XRD) points assume either the ambient BCC phase or ω-phase. (b) The appearance of an additional Ta peak for pressures above 340 GPa is consistent with a transition to ω-phase predicted by Burakovski (2010). To the best of our knowledge, this is the highest-pressure solid-solid phase transition observed to date.*

Hohlraum Diffraction (HohlDiff-11A, PI James Hawreliak)

In situ x-ray diffraction (XRD) provides a unique measurement of atomic arrangement that help us determine the materials lattice structure and phase, which are key components of understanding a materials equation of state (EOS). There are many scientific and programmatic objectives that will use XRD as a means of understanding the high pressure state, the current materials IET platform on NIF will use a hohlraum drive to load the sample, our current diffraction techniques may not be compatible with a hohlraum drive or other planned high pressure materials experiment on NIF and

Omega. The objective of HohlDiff 11A is to test an energy dispersive diffraction technique on the Omega EP laser system which may be compatible with a hohlraum drive.

The energy dispersive diffraction technique uses a fixed experimental geometry, with a broadband x-ray source. The relative angle between the x-ray source and detector fixes the angle, θ , in the Bragg equation, $\lambda=2d\sin\theta$. Then peaks in the scattered energy will correspond to lattice plane spacing, d. This technique has the advantage that the detector can be remote from the sample and x-ray source and because the energy spectrum of the drive can be measured separately it can be spectrally separated from the diffraction signal. We used the L and M shell emission from a cocktail backlighter source to generate a quasi-broadband x-ray spectrum, and used the signal photon counting diagnostic on the Omega EP laser system as our energy dispersive detector.

Figure 1 is the energy corrected scattering data from the experiment. The black line is the backlighter when there is no target sample. The low energy signal suggests we need to do a better job in isolating the region viewed by the detector. The remaining three traces are different shots using different backlighter energies and filtering on the detector. There is a very strong peak at ~6.4keV which is most likely due to the fluorescence of the iron target sample. There are weaker peaks that begin to fall into the signal to noise which are consistent with XRD. We can use these results from the current configuration to determine a better experimental configuration that will yield higher diffracted photons on the detector.

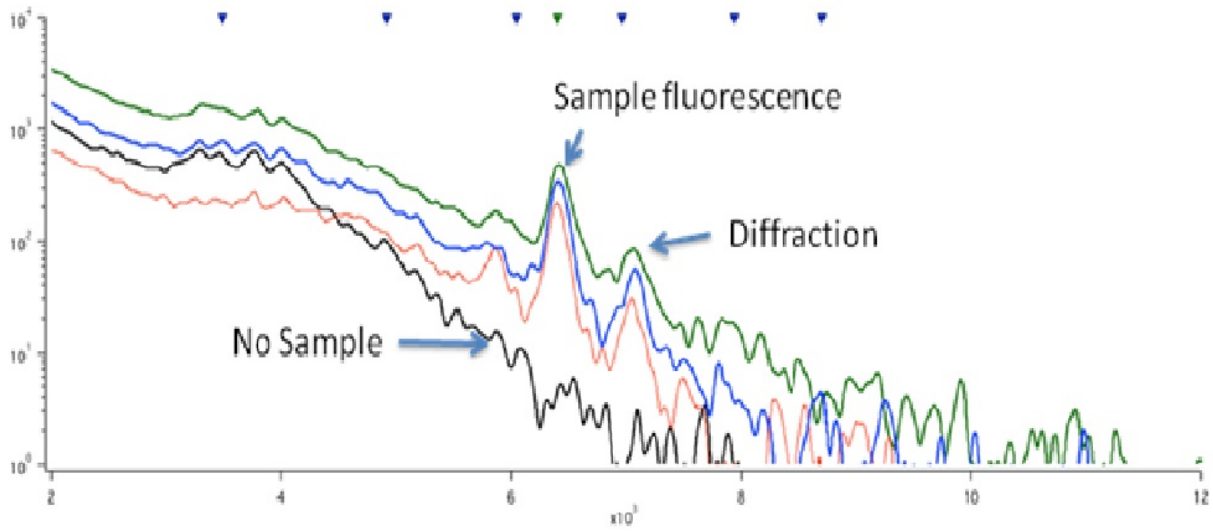

***Figure 1**: The energy corrected single photon counting data from the experiment. The black line is the backlighter when there is no target sample.*

Equation of state for Foams (FOAM EOS 11A11B PI James Hawreliak)

Low density foams are being used and planned to be used as materials in complex integrated experiments to model astrophysical phenomena, particularly for the formation and growth of density driven hydrodynamic instabilities. The shock response of the low-density foam is very important to the modeling, developing and interpretation of these experiments. While velocimetry techniques have been used to measure the shock speed in transparent foams the is a programmatic and scientific need to get Hugoniot equation of state in opaque carbon based foams. To do this we will use in situ radiography to measure the shock speed and shock density along with the Hugoniot conservation relations to determine the EOS.

The experiment used 16 beams to generate a Ti k-shell backlighter and four stacked beams to generate ~10ns drive. When the shock has propagated 10ns into the target we recorded multiple radiographs over 1ns using an x-ray framing camera. Figure 1a) is a VISRAD representation of the experiment.

Unfortunately due to the hot temperatures we were only able to get two shots, but the data shown below in Fig 1b) is of excellent quality. The data is currently being analyzed but a first calculation of the shock speed is ~20km/sec.

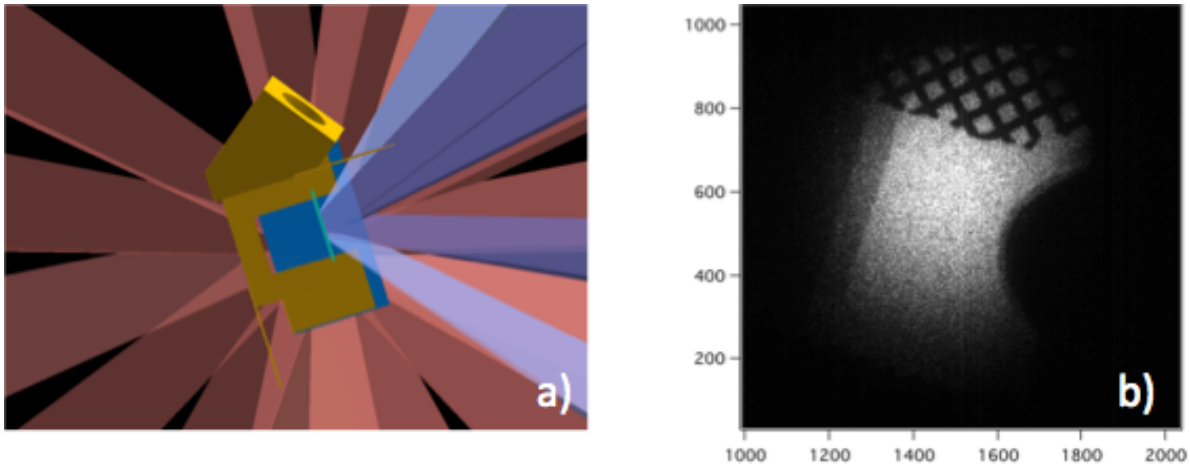

Figure 1: *a) A VISRAD model of the experiment from a TIM4 view b) a radiograph taken using an XRFC on TIM4.*

Gigabar Equation of State (GbarEOS-11A, PI James Hawreliak)

The high energy density (HED) physics regime is where the energy density of a system is comparable to the binding energy density of a Hydrogen molecule, i.e. ~1Mbar. We can define an atomic unit of pressure in the same fashion as the ground state energy density of a hydrogen atom, which is ~300Mbar. As we approach in the atomic unit of pressure we would begin to expect the core and inner shell electrons to be perturbed by the applied pressure. This will lead to novel chemistry and interesting science at high pressures. To achieve these high pressures we use a convergent spherical geometry. Unlike a planar target the applied shock pressure increases in strength as it approaches the center.

The experiments performed on the Omega laser used 40 beams on the P6-P7 axis in a hohlraum to indirectly drive a converging shock into a spherical capsule of PAMS. Two backlighters were used to investigate the shock wave in the solid capsule. A gated framing camera on the P6-P7 axis was used to capture images, while an x-ray streak camera recorded a time resolved radiograph on the axis of the capsule. Figure 1a) shows a VISRAD view of the target configuration. In this configuration we can measure the equation of state by getting two points on the Hugoniot, the shock speed from the time resolved measurement and the density from the radiograph.

Figure 1b) shows radiograph images of the shock wave in the capsule at two different times. These were taken after the drive beams have been turned off because of the x-ray signal from the hohlraum overwhelmed the radiograph signal. We see clear evidence of the shock wave propagating into the capsule, while analysis is on going we get an estimate of the shock speed of 80km/sec.

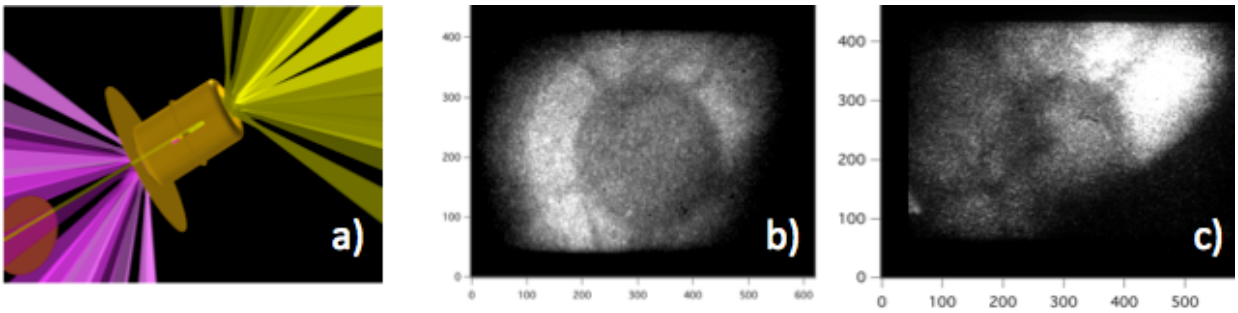

Figure 1*: a) A VISRAD model of the experiment b) a radiograph of the capsule c) radiograph 1ns later.*

Double Pulse (DblPulse-11A/B PIs Brian Maddox, Andrew Comley)

The goals of this campaign were to measure the sensitivity and MTF of the x-ray framing camera at 8 keV and 22 keV and to measure the conversion efficiency of a Cu microflag x-ray source using a 100 ps UV pulse. To measure the sensitivity of the XRFC used Cu and Ag backlighters and placed filters in front of both the HERIE detector, on TIM13 and the XRFC, on TIM 10. The filters consisted of a Ta mask and sets of filter steps placed over holes machined into the Ta mask. For the Cu shots, the filters were Cu and Al steps, and for the Ag shots the filters were Ag and Ta steps with an additional Mo/Pd Ross pair. For the resolution tests, targets consisted of double-ended Au resolution grids aimed at TIM 13 and TIM 10 that were backlit using 5 um thick Cu and Ag microflags. After a slow start and an issue with one of the TVS shutters, we were able to obtain high-quality data on all shots, resulting in data that will be used to calculate the sensitivity and resolution of the XRFC at 8 and 22 keV. Figure 1 shows a sample image from s10050 of the Au grid projected onto a single-strip XRFC using a 22 keV Ag backlighter. We also obtained very good conversion efficiency data using the single photon counting camera (SPC) for the 100 ps UV pulse, finding that the conversion efficiency at 8 keV was only a factor of 2X lower than that using a 1 ns UV pulse, with CE = 3.5×10^{-3} for the 100 ps UV pulse.

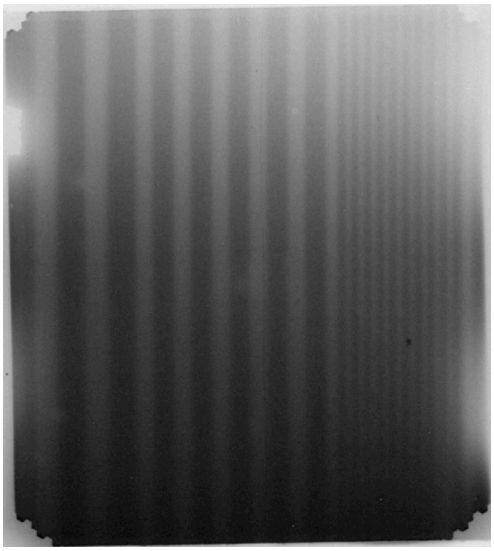

Figure 1: *Radiograph collected on a single-strip XRFC of a Au grid backlit using a 5 um thick Ag microflag.*

Dynamic and Lattice Diffraction (LattDyn-11A/B, DynDiff-11A, PI Brian Maddox)

The goal of these campaigns was to develop Bragg diffraction using a Petawatt backlighter and to study single crystal Mo shock-compressed along the [111] direction using angle-dispersive Bragg diffraction. These campaigns saw a drastic improvement in the quality of Bragg diffraction obtained using a Petawatt backlighter primarily due to the high-quality surface polish conducted at LLNL to remove a thick layer of damage from the rough manufacture polish and due to a new improved beam block design. Bragg diffraction requires one to block the x-rays directly from the x-ray source while allowing the diffracted x-rays to pass. In these experiments the backlighter was a 250 um diameter, 12 um thick Mo foil driven using the Omega EP backlighter beam, defocused to 200 um and using a 100 ps pulse length. The new beam block design is specially shaped to avoid exposed corners, which are able to produce strong self-emission. The new design is also much closer to the x-ray source, effectively block all of the direct x-rays while allowing the use of xtvs and ytvs for positioning. A representative diffraction image is shown in Fig. 1. Evidence in this image are the diffraction lines from the shocked lattice and the unshocked lattice in front of the shockwave. The strong lines are diffraction 17 keV Mo Kα x-rays while the faint lines are diffracted Kb x-rays. Data was spanning all three campaigns resulting in shock-compressed Mo data from 10 GPa to 40 GPa. A transition from elastic compression to plastic flow was observed at ~15 GPa. The diffraction data has been analyzed to extract the yield stress and the von Mises stress. We also observed plastic relaxation times << 1 ns above 15 GPa. These results are currently being prepared for publication.

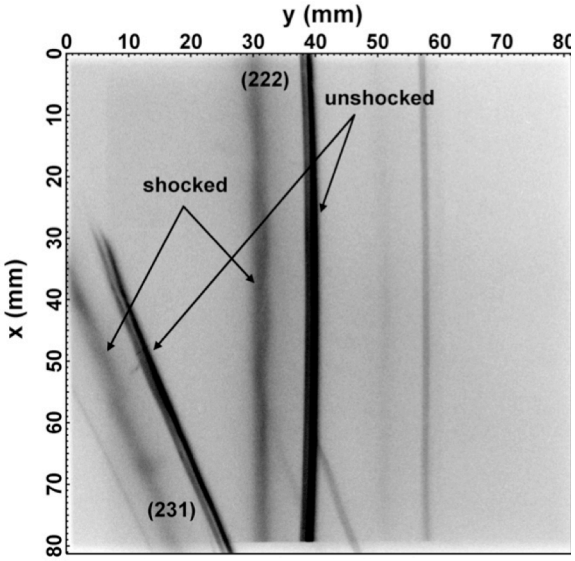

Figure 1: *Laue diffraction pattern obtained from single crystal Ta shock along the [001] direction using 20.6 J, 1ns long UV laser drive*

Tantalum Rayleigh-Taylor Experiments (ICETaRT-11A, PI Hye-Sook Park)

The goal of the ICETaRT campaigns is to measure dynamic properties of solid-state tantalum (Ta) under high pressures (>1 Mbar) and high strain rates (10^6 - 10^8 sec^{-1}). We achieve quasi-isentropic high-pressure conditions by utilizing a unique reservoir-gap-sample configuration where the sample materials stay well below the melting temperature while they are plastically deforming under high pressure as shown in Figure 1. This year's campaign studied tantalum material strength properties under these conditions by measuring the growth due to the Rayleigh-Taylor (RT) instability in

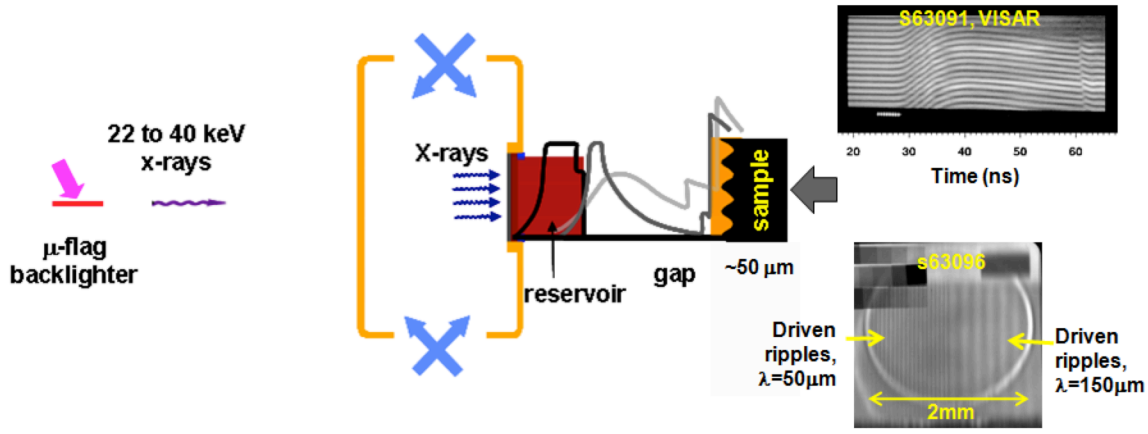

Figure 1. *ICETaRT experiment configuration for a Omega/Omega-EP joint shot. We take 2 types for data on each set: Drive data using the VISAR and face-on radiography using the EP generated high energy backlighter.*

accelerated samples containing a pre-imposed sinusoidal ripple. We obtain 2 types of data from each set: drive measurement using the VISAR and the face-on radiography using the 20 keV Ag K-α backlighter via Omega-EP short pulse laser. We have obtained a series of successful radiography over these campaigns. The radiometrics of the Ta stepped data are carefully analyzed to derive the ρΔZ of the ripple growth. The growth factor, GF, is then defined to be:

$$GF = \frac{(\rho\Delta Z)_{driven}}{(\rho_0\Delta Z_0)_{undriven} \cdot MTF}, \qquad (1)$$

where ρ_0, ΔZ_0 are initial density and ripple amplitude from the pre-shot metrology and MTF is modulation transfer function measured by the knife-edge. Figure 2 shows the ripple growth factor as a function of time from the 50 μm wavelength samples. The simulation results from various material strength models are also plotted in Fig. 2. Note that only the multiscale model fits the data well which attempts to connect atomistic level behavior to the continuum level plastic flow utilizing density functional theory, molecular dynamics, dislocation dynamics and continuum simulations to calculate yield strength.

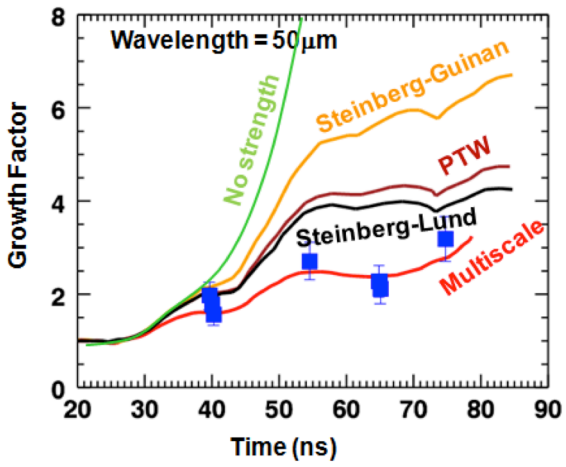

Figure 2. *Ta Rayleigh-Taylor growth factors as a function of time. The data points are noted as the blue squares. Various material strength model predictions are plotted.*

The details of this model are described in Ref. [1].

Flow stress is the stress that is needed for the metal material to flow plastically at a given loading condition and state. The inferred average flow stress using the multiscale model, averaged over the sample with e^{-kz} weighting (where $k = 2\pi/\lambda$, and z is the depth into the foil), is ~60 kbar which is ~8 times higher than the Ta ambient flow stress of 7.7 kbar. We find that the flow stress is largest when the strain rate is the largest, indicating the strain rate hardening is a dominant factor. From the pressure-dependent shear modulus calculation, the pressure hardening is about a factor of 2, with the remaining factor of 4 due to strain rate hardening. This result is submitted and accepted for a publication [Ref. 2]

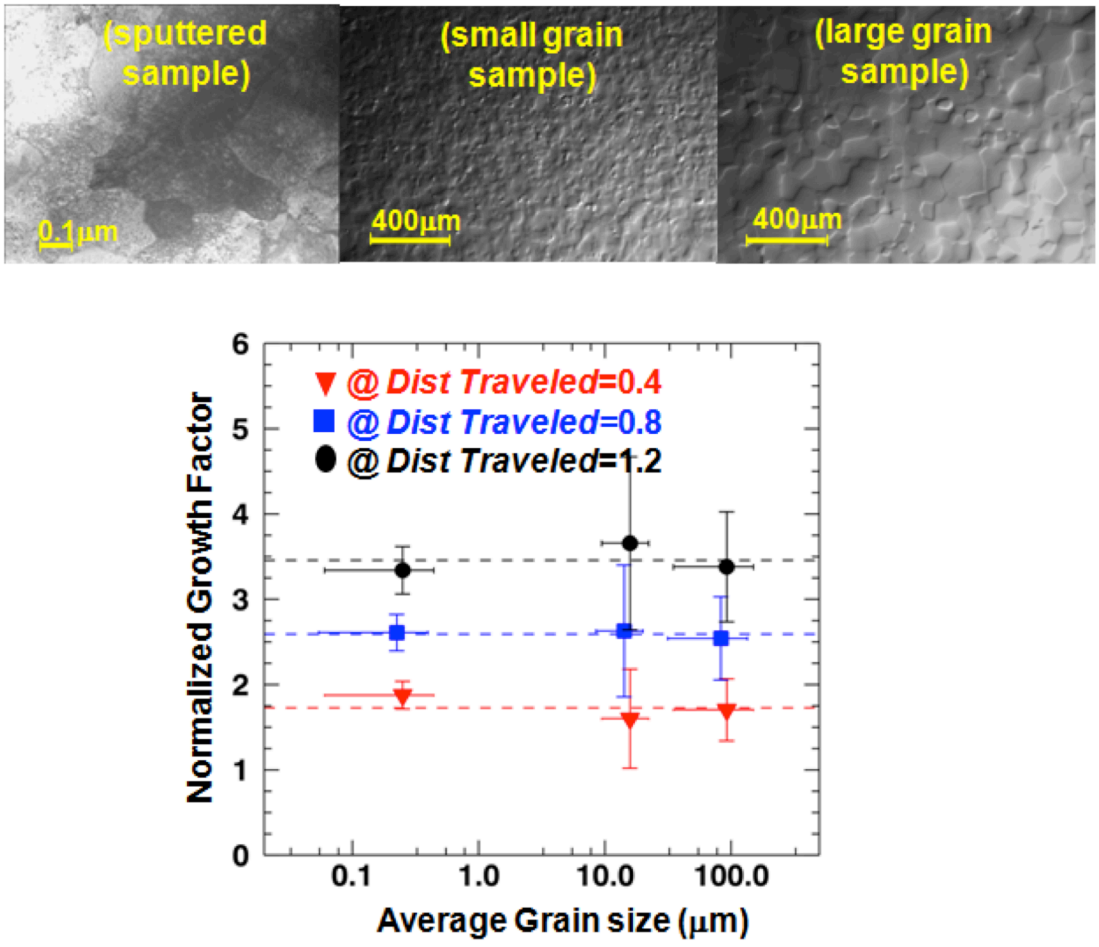

Figure 3: *(a) SEM and TEM pictures of the different Ta grain size samples. (b) Growth factor, a measure of material strength, as function of grain size. No obvious Hall-Petch effect is observed.*

FY11 campaign also completed a study of the Ta grain size effect on the strength under high pressure and high strain rate conditions. While there are many strength measurements of Hall-Petch grain size scaling at ambient conditions, neither previous theory nor experimental measurements under high-pressure dynamic conditions exists. We fabricated 3 different types of target that have average grain sizes of 92 μm, 15 μm and 0.25 μm as shown in Figure 3 top panel. The face-on radiography data are analyzed in the similar fashion described above and the normalized growth factor vs. the average grain size is plotted in the bottom panel of Fig 3. The conventional understanding is that the yield strength is stronger with smaller grain sizes known as the Hall-Petch

effect and is formulated by: $\sigma \sim \sigma_0 + kD^{-1/2}$, where σ is the yield strength, D is the average grain size diameter, σ_0 and k are characteristic coefficients for different materials. This relation is known to be holding for many materials. This is explained by the dislocations, whose mobility quantifies the strength, are pinned against the grain boundary restricting their mobility. We consider two postulations why we don't see the Hall-Petch effect: 1) that in our experiment, the dislocations have not moved to the grain boundaries at our times scale of <100 ns; 2) that the work hardening is a dominant factor rather than the grain size hardening. Our experimental results will be submitted to a publication to Nature-Material journal.

[1] N.R. Barton et al., J. Appl. Phys., **109**, 073501 (2011).
[2] H.-S. Park et al., "Experimental results of Ta material strength at high pressure and high strain rate", accepted a publication in AIP for the SCCM proceedings (2011).
[3] H.-S. Park et al., "Tantalum material strength dependence on grain sizes at 100 GPa pressure and 107sec-1 strain rates", in preparation.

ICEDrive-11A / ICEHohl-11A (PI: May / Comley)

The ICEDrive-11A and ICEHohl-11A campaigns were conducted at the OMEGA laser facility as part of the ramped-drive platform development required for the tantalum strength Rayleigh-Taylor experiment on NIF. Both half-day campaigns were fielded on the same day and used the 2.5-scale indirect-drive platform developed in the ICETaRT series of experiments, with slight variations in the drive package design to address various issues as described below.

The ICEDrive-11A target packages are shown in Fig. 1. The hohlraum drive is incident on the beryllium ablator shown in the figure. The BrCH (and foam layers if applicable) constitute the reservoir that releases across the gap, thereby generating a ramped pressure wave at the tantalum

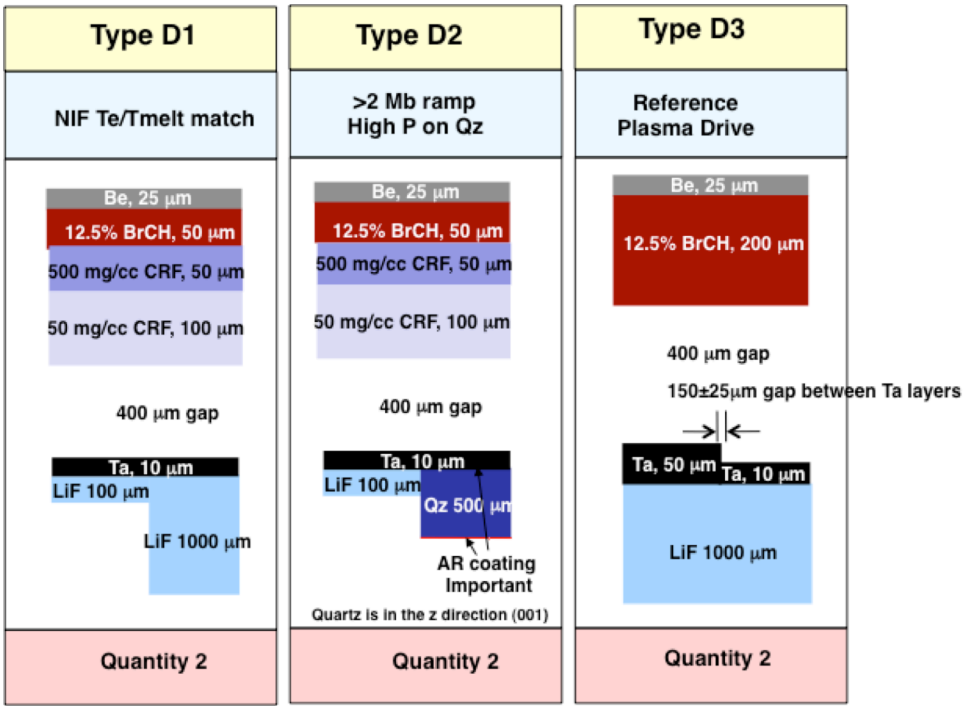

Figure 1: *ICEDrive-11A target packages.*

layer. The ramp drive is characterized using VISAR and SOP. The ICEDrive-11A experiments were designed to test VISAR measurement handoff from thin (100um) LiF to thick (1mm) Quartz at pressures >2 Mbar (a key component of the NIF 5-Mbar drive target designs), test two-layer reservoir foam repeatability, provide further experience with diagnosing the drive through a releasing LiF reservoir, and provide a reference drive shot for the ICEHohl-11A experiments later in the day.

All six targets shots returned good data from primary diagnostics VISAR, Dante and SOP. The peak drive Tr measured from Dante is currently higher by 3-8 eV than previous campaigns. The drive (deviating in the opposite direction) as measured by VISAR is lower by ~15%.

The ICEHohl-11A target packages are shown in Fig. 2. The ICEHohl-11A experiments had two

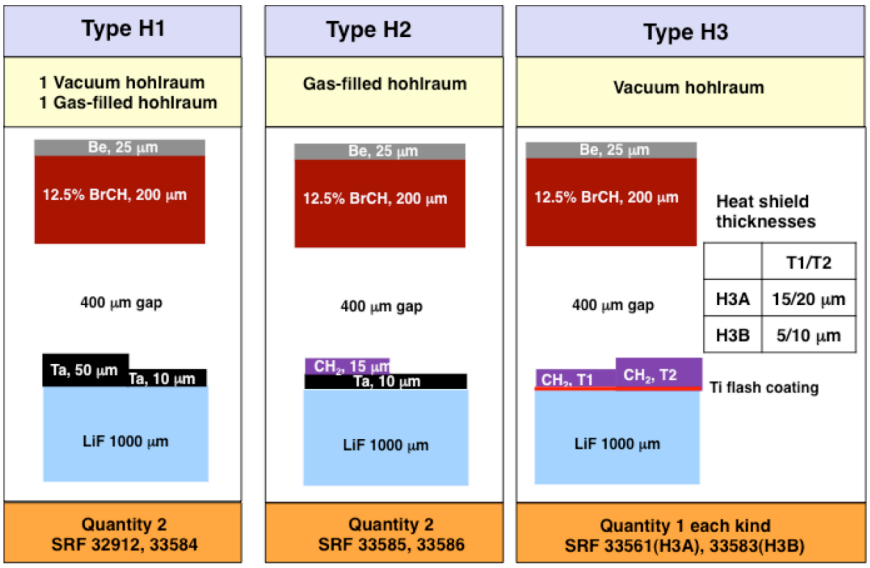

Figure 2: *ICEHohl-11A target packages.*

objectives. Firstly, in the tantalum strength Rayleigh-Taylor experiment (ICETaRT), a plastic (CH2) heat shield is placed over the front of the tantalum sample in order to insulate it from the heating effects of the unloading reservoir. The ability of CH2 to act as a thermal insulator to the stagnating plasma in a planar geometry was demonstrated (H3 target in Fig. 2) using streaked optical pyrometry. No thermal burnthrough was observed, in agreement with tabular electron conductivity values.

The second objective was to test the performance of gas-filled hohlraums, particularly with a view to mitigating late-time shock formation due to hohlraum stagnation and late-time Tr effects. We tested three neopentane-filled hohlraums, with nominal gas pressures of 26, 129 and 180 Torr. It was found that the timing of the late-time shock could be influenced by choice of gas fill. For increasing gas fill pressure, the late-time shock was observed to arrive earlier: the shock time measured relative to the start of the initial ramp for the 180 Torr case was seen to shift ~4ns earlier compared to the 129 Torr case.

Strength Diffraction (StrDiff-11A, PI Brian Maddox)

The goals of this campaign were to study single crystal Ta shocked along [001] using Laue diffraction and to measure the broadband output of a 1 ns UV pulse driven foil source to that of a 44 beam imploded CH shell source using the DCS. This campaign was also used to test a new Ta crystal target build scheme to keep the 5 um thick Ta single crystals as strain-free as possible. Laue diffraction was obtained using the BBXRD diagnostic on TIM4. DANTE was used to time the capsule implosion for precise timing between the Ta crystal drive and the x-ray bang time. The results show that the new target construction scheme using a 10um n-HDC ablator glued to a Ta crystal with a 40um thick u-HDC tamper effectively kept the Ta crystal from warping and produce high-quality static and shocked diffraction patterns. Figure 1 shows a sample diffraction pattern from one of the image plates of the BBXRD from a Ta sample driven using 20.6 J in 1 ns. Evident in the image is are diffraction spots from the shock-compressed lattice and the unshocked lattice ahead of the shockwave. The particular image corresponds to a 9% difference between the longitudinal and lateral strains. High quality data was also obtained on the broadband spectrum of a Mo foil backlighter driven using 4 UV beams at max energy with 1ns pulse lengths, overlapped in space and time onto a 1mm diameter, 12.5 um thick Mo foil. The results showed that the broadband emission of the Mo foil in the 10-20 keV range was ~10X lower than that from the imploded CH shell backlighter. Subsequent campaigns will continue to use the CH shell as the broadband x-ray source for Laue diffraction.

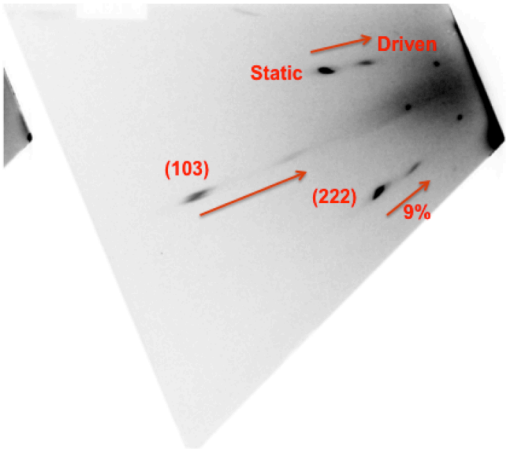

***Figure 1**: Laue diffraction pattern obtained from single crystal Ta shock along the [001] direction using 20.6 J, 1ns long UV laser drive*

II. High-Temperature Plasma Opacity

High-Temperature Plasma Opacity Experiments on Omega and Omega-EP (PI: R.F. Heeter with S. Chen, G.V. Brown and R.E. Marrs)

LLNL opacity research in FY11 had four main directions. First, the MBOP-11 campaign followed up on physics questions from the very successful 2009-10 Ti opacity shots, where the observed Ti continuum opacity and 1-3 line opacity regions did not match code expectations. The new data using thinner samples extended this dataset by a factor of 4 in sample rho-L, pushing the K-shell absorption technique to its optically thin limit. As shown in Figure 1, spectral absorption line positions from charge states consistent with ~120 eV LTE sample temperatures are observed, now with 40% transmission. The new data continue to match the codes quite well, and detailed comparisons are in progress for the continuum and line-gap opacities where disagreements with the older data remain.

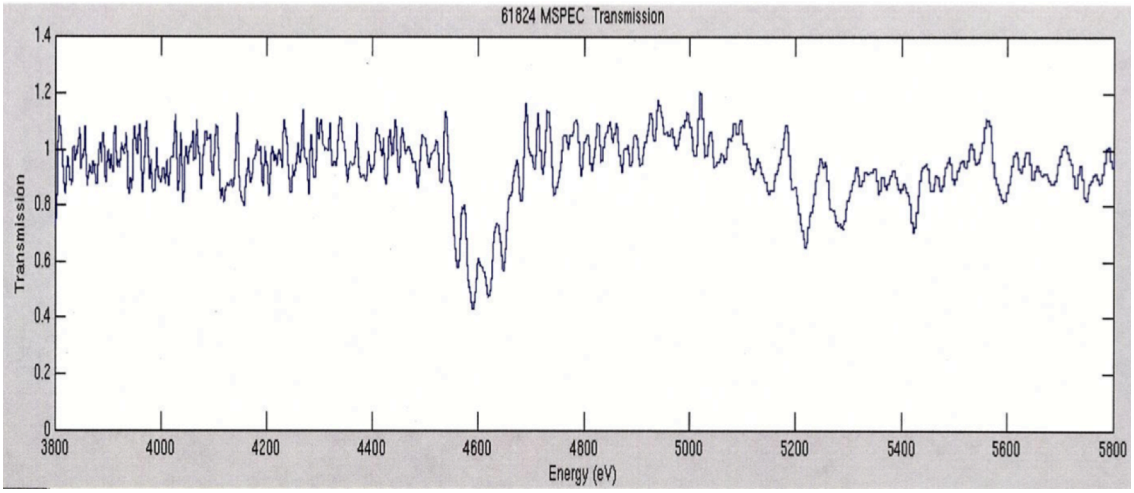

***Figure 1**: Ti K-shell transmission spectrum with 0.17 um Ti sample. Foil expanded to 70 um from initial 0.17 um. Sample thickness reduced 4x from earlier experiments, bringing K-shell features to >40% transmission. Ionization features for F, O, N and C-like Ti indicate temperature of 120 eV.*

The second campaign, NEAHiZ-11, resumed previous work on the non-LTE X-ray emission properties of hot gold plasmas as found in hohlraums at the laser-driven "hot spots". Shots performed in late FY11 extended earlier work to 2x lower intensity (material temperature) and the data are now being compared with simulations.

NEAHiZ-11 also supported a third line of inquiry to improve the signal/noise of gated opacity measurements. As part of the non-LTE measurements, the relative sensitivity of XRFC1 (50 ps PFM) was compared with XRFC4 (new MCP, 400 ps PFM); the latter showed roughly 300 times greater sensitivity for X-rays from 250-1800 eV, using nearly identical snout setup and target views. The noise in both measurements is similar (hence, not photon-limited) and subsequent investigations established a signal/noise limit of 20:1 for film-based gated X-ray imaging with 60-100 um-spatial resolution. This ratio is limited by the film itself, and not the scanner or XRFC components. The ratio may be increased by averaging over wider sections of film, or perhaps by modifying the film developing process.

The fourth research direction was the EPOp-11 series, which successfully developed a novel short-pulse "absorption-emission" opacity platform on Omega-EP. The initial goal was to crosscheck short-pulse heated opacity measurements against similar long-pulse data (Ti, T≈100-150 eV, density ~0.05-0.2 g/cm^3). Absorption experiments at higher densities and temperatures are possible, but maintaining LTE conditions is difficult. In the FY11 experiments, the EP sidelighter beam delivered 250-900J in 100 ps with a broad focus to heat Al/Ti/Al2O3 opacity samples at 10^15-10^16 W/cm^2 intensities. The EP backlighter beam, delayed 200-300 ps, delivered 800-1500J in 10 ps near best focus, driving a broadband 3-6 keV backlighter whose X-rays probed the hot, expanded opacity sample. Figure 1 shows K-shell X-ray absorption from L-shell Ti ions (F, O and C-like Ti) at T > 100 eV. The inferred temperature is below the ~1000 eV temperatures predicted by the 1-D hydrocode HELIOS and HYDRA. Imaging in the transverse direction shows an expansion of ~50 um (density of ~0.05 g/cc) at the time of this measurement. A separate line of sight allowed space- and energy-resolved sample emission spectra to be taken in the 250-1600 eV spectral band, which shows similar levels of expansion and ionization.

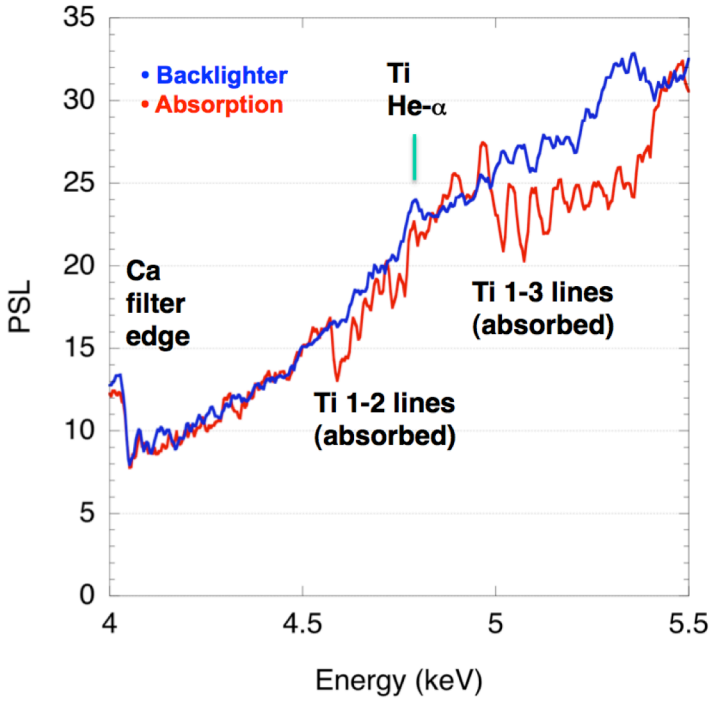

Figure 2: *First Ti K-shell absorption spectrum from EP Opacity experiments. Similar charge states are seen in the EP experiment as in the Omega experiment.*

III. Hydrodynamics

Short-pulse, UV backlighting development for NIF (InvCasc-11A, PI: Vladimir Smalyuk)

High-Energy-Density Complex Hydrodynamics experiments on National Ignition Facility (NIF) require short-pulse backlighting capability. Experiments on OMEGA-EP laser tested short-pulse, UV beam backlighting concept for NIF. Four OMEGA-EP beams were focused onto 10-μm thick Ag wires, mounted on 300 x 300 μm square, 10-μm thick polyimide foils to mimic illumination conditions of one quad on NIF. Total laser energy was ~400 J with ~100 ps Gaussian pulse shape and peak laser intensity of ~$3x10^{16}$ W/cm^2. Beam mistiming was <50 ps rms, and mispointing <50 μm rms. Results were compared with ~1.2 kJ short-pulse (~100 ps) IR beam backlighting with the same Ag-wire targets, driven at intensity of ~$1x10^{17}$ W/cm^2. Figure 1 shows a measured image of the target, created with Ag-wire backlighting on an image plate using HERIE diagnostic located at 50 cm from target chamber center on OMEGA-EP. It consists of the Au grid, used to determine magnification, 100-μm thick Au plate, used to determine resolution, and seven Cu steps with 18 μm thickness between adjacent steps, used to determine contrast and sensitivity. Areas inside and outside of Au plate were also used to measure noise. Figure 2(a) shows inferred backlighter spectrum, determined by fitting measured intensity in Cu steps, shown in Fig. 2(b) with diamonds.

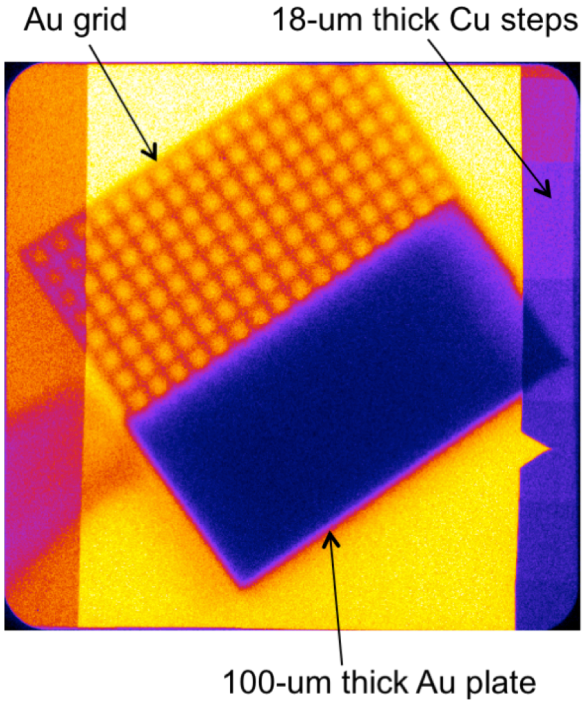

Figure 1: *X-ray radiograph of the target consisting of Au grid, 100-μm thick Au plate, and seven 17-μm thick Cu steps.*

Thick solid line shows a fit to the data assuming an exponential backlighter x-ray spectrum with temperature of 13±2 keV, presented in Fig. 2(a). The inferred temperature was ~100 times lower than in experiments with short-pulse IR beam, while signal intensity in the areas outside of the Cu steps (about 2 PSL) was decreased by ~100 times. The spatial resolution of ~20 μm was similar to IR-beam experiments, while noise was ~2 times higher. The short-pulse UV backlighting might be feasible for Complex Hydrodynamics experiments on NIF if hohlraum x-ray backgrounds (generated by mostly hot electrons from Raman laser-plasma instability) do not exceed ~10 PSL on the image plate at 50 cm from NIF target chamber center. First Complex Hydrodynamics experiments on NIF will measure and mitigate, if necessary, these backgrounds before radiography experiments. Next campaign on OMEGA-EP will be devoted to maximizing x-ray backlighter signal by scanning a temporal advance of one of the beams with respect to other drive beams.

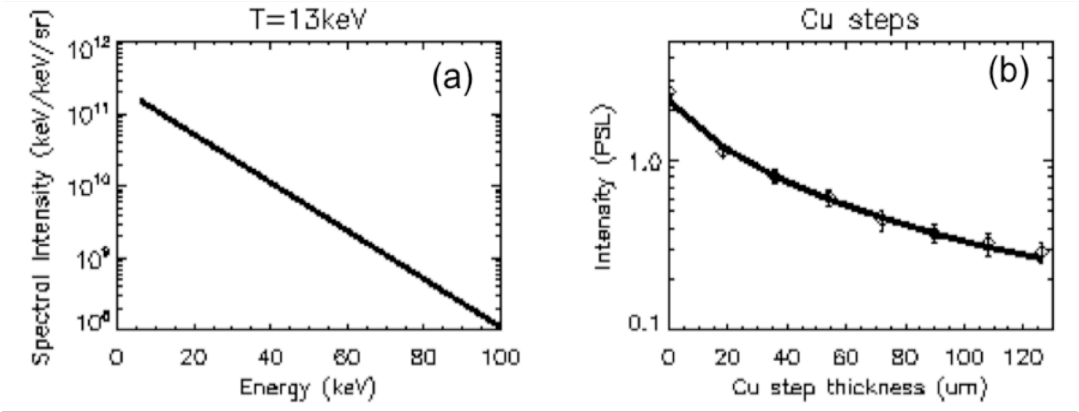

Figure 2. *(a) Inferred backlighter spectrum, determined by fitting measured intensity in Cu steps, shown in (b) with diamonds. Thick solid line shows a fit to the data assuming an exponential spectrum with temperature of 13±2 keV, presented (a).*

Backlighting experiments on OMEGA (Toto-11B, PI Vladimir Smalyuk)

Backlighting experiments were performed on OMEGA laser system to study symmetry of the foam balls illuminated with hohlraum x-rays. Backlighter targets were driven either with short-pulse IR beam in a Joint OMEGA-EP experiments, or with UV beams in OMEGA-only experiments. In a Joint OMEGA-EP configuration, 10-μm thick Ag wires, mounted on 300 x 300 μm square, 10-μm thick polyimide foils were irradiated with ~1.2 kJ short-pulse (~100 ps) IR beam at laser intensity of ~$1x10^{17}$ W/cm^2. X-ray radiographs of targets were measured on image plates using HERIE diagnostic placed at ~50 cm from target chamber center with magnification of ~50. In OMEGA-only configuration, six OMEGA beams irradiated Ni point-projection backlighter at laser intensity of ~$1x10^{16}$ W/cm^2. Time resolved (with ~80 ps temporal resolution) x-ray radiographs of targets were measured on a framing camera with magnification of ~20. Experiments were very successful, they produced high-quality radiographs that set up a baseline for future Complex Hydrodynamics experiments on National Ignition Facility (NIF).

IV. X-Ray Source Development and Application

Iron K-shell X-ray Source Development (FeKshell-11A/B, PI Kevin Fournier)

The X-ray Source Development team, in collaboration with the Defense Threat Reduction Agency and researchers from the French CEA, conducted two campaigns in FY11 that developed

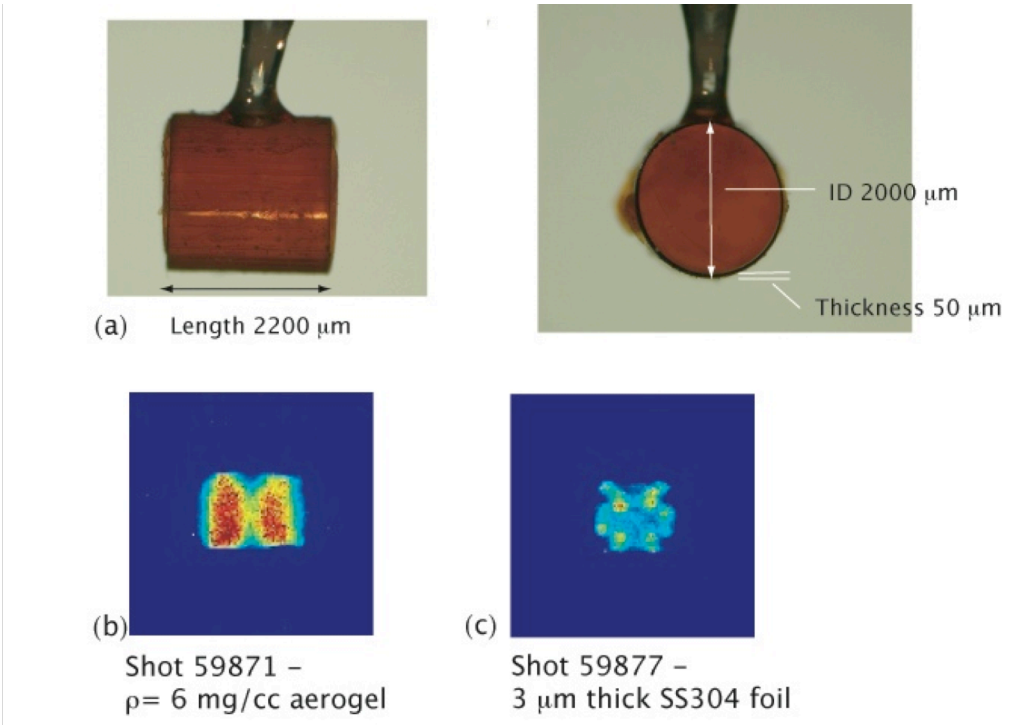

Figure 1 *– (a) Side-on and face-on views of a 12 mg/cm3 iron-oxide aerogel target for FeKshell-11A shots, and (b) x-ray framing camera (XRFC) image at 6.7 keV x-ray energy of a 6 mg/cm3 aerogel target at t=1.0 ns, and (c) XRFC image at 6.7 keV x-ray energy of a 3 mm thick steel-lined cavity at 0.8 ns. The Fe K-shell emission from the aerogel target is much brighter than from the foil-cavity target.*

and optimized two very different iron K-shell x-ray sources with x-ray emission principally at 6.7 keV. The two sources that were studied were ultra-low-density iron-oxide aerogel materials ($FeOOHCl_{0.38}$) and stainless-steel-lined (SS-304) cavities, see Fig. 1. The density of the aerogel targets ranged from 3 – 16 mg/cm^3, which resulted in laser-created plasma radiation sources with densities between 10 – 50% of the OMEGA laser's critical density. The critical measurements that were made include x-ray spectral output from the sources, x-ray images of the volume heating of the target plasma, and streaked images of laser heating in the targets. Side-by-side images of the heated aerogel and foil-lined cavity targets are shown in Fig. 1. Results so far show that the aerogel material at 6 mg/cm^3 produced the highest fluence 6.7 keV output at 43.1±9.4 J/sr, which is a 2.9% laser-to-x-ray conversion. The Fe K-shell yield (6 – 8 keV) of the aerogel targets for three different densities is shown in Fig. 2. When measured over all x-ray energies, the targets yielded ≈850 J/sr and ≈1220 J/sr for aerogel and steel-lined cavities, respectively. These targets show promise for reproducible, high-flux, high-fluence x-ray sources to be used in NIF experiments in FY12 and beyond.

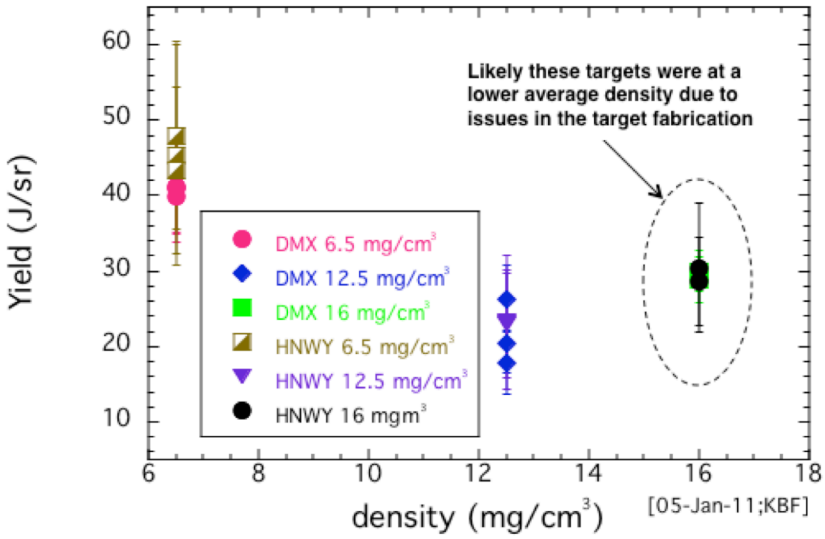

Figure 2 *– Measured Fe K-shell yields in the energy range 6 – 8 keV for iron-oxide aerogel targets of different densities. The measurements were taken with the CEA diagnostic DMX and the LLNL diagnostic HENWAY; the two diagnostics show excellent agreement.*

Solar Cell Electrostatic Discharge (SolarCellESD-11A, PI Kevin Fournier)

The X-Ray Source Development team, in collaboration with the Naval Research Laboratory and the Defense Threat Reduction Agency, has begun researching whether we can use the OMEGA target chamber as a test environment for investigating electrostatic discharge phenomena in solar cell technology. Our initial steps in this process are to characterize the charged-particle flux (both electrons and ions) created by our laser-driven x-ray source before moving on to more sophisticated tests of biased solar cells and solar-cell arrays. Our first experiments, on 14 September, 2011 involved the fielding of arrays of Langmuir probes in TIMs that looked at the open face of our x-ray source targets and that looked orthogonal to the target's axis. The two lines of sight provided quantitative measurements of x-ray driven signals on a nanosecond time scale and electron and ion signals on the microsecond time scale. A photograph of one of our probe arrays is shown in Fig. 1. The Langmuir probe diagnostic is a new diagnostic created by modification of the X-Ray Source Application (XRSA) cassette that we've used on many previous radiation-effects experiments. We will return to the development of this platform in FY12 with arrays with a greater number of probes on each shot that will allow us to map out the voltage-current curve for the passing ion and electron fluxes, and, ultimately, an investigation of the response of a solar-cell array operating under bias to x-ray loading.

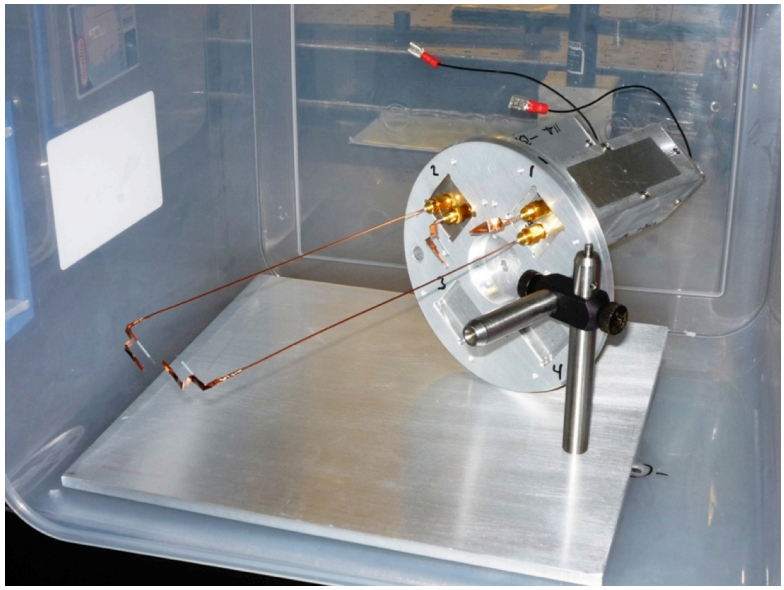

Figure 1 *– A XRSA cassette fitted with two sets of Langmuir probes ready for delivery to the TIM for positioning in the OMEGA laser chamber. The probes measure electron and ion particle fluxes passing by their location following laser-irradiation of the x-ray source target at TCC.*